nature geoscience

ARTICLES

https://doi.org/10.1038/s41561-022-01017-x

Check for updates

OPEN

Carbon and sediment fluxes inhibited in the submarine Congo Canyon by landslide-damming

Ed L. Pope[1]✉, Maarten S. Heijnen[2,3], Peter J. Talling[1], Ricardo Silva Jacinto[4], Arnaud Gaillot[4], Megan L. Baker[1], Sophie Hage[5,6], Martin Hasenhündl[7], Catharina J. Heerema[1,8], Claire McGhee[9], Sean C. Ruffell[1], Stephen M. Simmons[10], Matthieu J. B. Cartigny[1], Michael A. Clare[2], Bernard Dennielou[4], Daniel R. Parsons[10], Christine Peirce[1] and Morelia Urlaub[11]

Landslide-dams, which are often transient, can strongly affect the geomorphology, and sediment and geochemical fluxes, within subaerial fluvial systems. The potential occurrence and impact of analogous landslide-dams in submarine canyons has, however, been difficult to determine due to a scarcity of sufficiently time-resolved observations. Here we present repeat bathymetric surveys of a major submarine canyon, the Congo Canyon, offshore West Africa, from 2005 and 2019. We show how an ~0.09 km³ canyon-flank landslide dammed the canyon, causing temporary storage of a further ~0.4 km³ of sediment, containing ~5 Mt of primarily terrestrial organic carbon. The trapped sediment was up to 150 m thick and extended >26 km up-canyon of the landslide-dam. This sediment has been transported by turbidity currents whose sediment load is trapped by the landslide-dam. Our results suggest canyon-flank collapses can be important controls on canyon morphology as they can generate or contribute to the formation of meander cut-offs, knickpoints and terraces. Flank collapses have the potential to modulate sediment and geochemical fluxes to the deep sea and may impact efficiency of major submarine canyons as transport conduits and locations of organic carbon sequestration. This has potential consequences for deep-sea ecosystems that rely on organic carbon transported through submarine canyons.

The largest canyons on our planet occur on the seabed[1], and the submarine flows that flush these canyons form the largest sediment accumulations on Earth[2,3]. Only rivers carry comparable amounts of sediment and organic carbon (OC) across such large areas[4,5]. However, unlike rivers, there are exceptionally few time-lapse surveys of submarine canyons. Only ~4 of 9,477 submarine canyons documented globally[1] have time-lapse surveys, and this is the first time-lapse survey of a submarine canyon feeding a large (>150,000 km²) submarine fan in the deep (2–5 km) sea. There are also few direct measurements of the flows that flush submarine canyons[6–9]. This ensures that rates of geomorphic evolution, and the associated sediment and geochemical fluxes, including OC, are far more poorly understood than those for rivers. Previous time-lapse surveys of the upper reaches of much smaller submarine canyons have identified channel migration[10], bedform movement[6,9] and landslides[11]. We use repeat mapping of the Congo Canyon to show how canyon-flank landslides can affect canyon geomorphology and fluxes of sediment and carbon to the deep sea.

Landslides are important geomorphic agents in terrestrial environments. Where landslides flow into river channels they can lead to full blockages (landslide-dams)[12,13], channel constrictions, diversions or avulsions of the river channel itself[12,14,15]. Once emplaced, the landslide-dam itself can fail instantaneously, leading to erosion and transport of sediment upstream and downstream of the dam[16]. Over longer timescales, and depending on their longevity, landslide-dams can result in the accumulation of sediments and organic material upstream of the dam[13,17,18]. Upstream aggradation and downstream incision can lead to knickpoint generation in river longitudinal profiles[19]. Frequent landslide-dams or large-magnitude events can therefore notably influence river profiles over long timescales[19]. From an ecological perspective, landslide-dams can impact water quality and aquatic habitats in rivers[12,13] and are a key phenomenon in fluvial landscape evolution.

In this Article, we show how landslide-dams can impact submarine canyons. Submarine canyons are carved by slope failures and sediment flows called turbidity currents that can run out for hundreds of kilometres[11,20]. Indeed, landslide scars are ubiquitous on submarine canyon walls in many locations worldwide[11,21,22], suggesting that landslide occurrence is common (see Supplementary Table 1). However, a nearly complete lack of repeat bathymetric surveys ensures their geomorphic effects and exact timing are poorly constrained. As a consequence, an a priori assumption often persists that these landslides commonly evolve from low-mobility slumps to higher-mobility flows and eventually turbulent turbidity currents[11,20]. Using repeat bathymetric mapping, we show how submarine landslides can impact canyon morphology and interact with turbidity currents in submarine canyons.

We then show how landslide-dams have the potential to affect the tempo of sediment and carbon transfer to the deep sea. Submarine canyons act as the primary conduits for sediment, oxygen, nutrient, pollutants and organic-matter transport from rivers and coasts to the deep sea[1,23–25]. They are commonly envisaged as highly efficient

[1]Departments of Geography and Earth Science, Durham University, Durham, UK. [2]National Oceanography Centre Southampton, Southampton, UK. [3]School of Ocean and Earth Sciences, University of Southampton, Southampton, UK. [4]Marine Geosciences Unit, IFREMER Centre de Brest, Plouzané, France. [5]Department of Geosciences, University of Calgary, Calgary, Alberta, Canada. [6]Univ Brest, CNRS, Ifremer, Geo-Ocean, Plouzané, France. [7]Institute of Hydraulic Engineering and Water Resources Management, TU Wien, Vienna, Austria. [8]Department of Geography, University of Victoria, Victoria, British Columbia, Canada. [9]School of Civil Engineering and Geosciences, Newcastle University, Newcastle upon Tyne, UK. [10]Energy and Environment Institute, University of Hull, Hull, UK. [11]GEOMAR Helmholtz Centre for Ocean Research, Kiel, Germany. ✉e-mail: edward.pope@durham.ac.uk

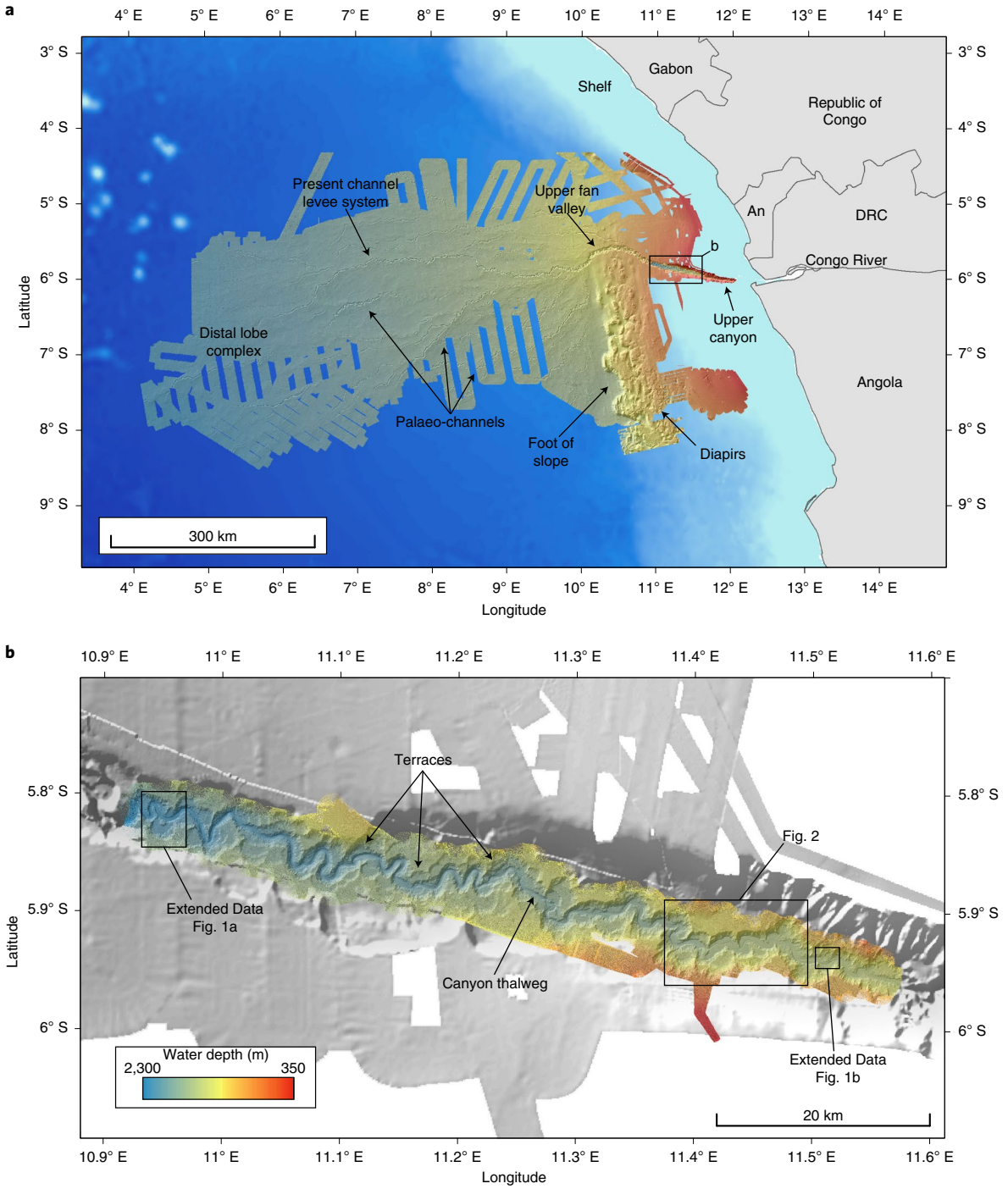

Fig. 1 | Study area and bathymetric map. a, Map of the Congo turbidite system. **b**, Bathymetry map of the upper Congo Canyon surveyed in 2019 on JC187. A sinuous canyon thalweg is present in the >800-m-deep canyon. Multiple terrace levels are also visible along the canyon. An, Angola; DRC, Democratic Republic of the Congo. **a**, Basemap from GEBCO; **b**, Congo Canyon/Fan bathymetry from Ifremer.

sediment transport conduits as well as locations for rapid burial and sequestration of substances such as OC[23,26,27]. It is therefore important to understand how landslide-dams, and their interaction with other sediment flows, can impact sediment and OC transfer through submarine canyons[28].

Congo Canyon and canyon-flank landslide-dams

The Congo Canyon, offshore West Africa (Fig. 1), is directly connected to the Congo River, the second-largest river by water discharge on Earth[4], and therefore acts as a continuous conveyor for sediment delivery from the river to the deep sea[22]. Annually, the river delivers ~43 Mt sediment and ~2 Mt OC into the canyon head, which is directly linked to the river mouth[29]. The canyon itself is 6–12 km wide and >800 m deep, and its floor is 50–800 m wide. The canyon walls have a largely concave pattern, with numerous individual headscarps recording past landslides[22,30] (Fig. 2a). There are also multiple terrace levels that are likely to be areas of high sediment accumulation and may be prone to collapse[31]. Monitoring

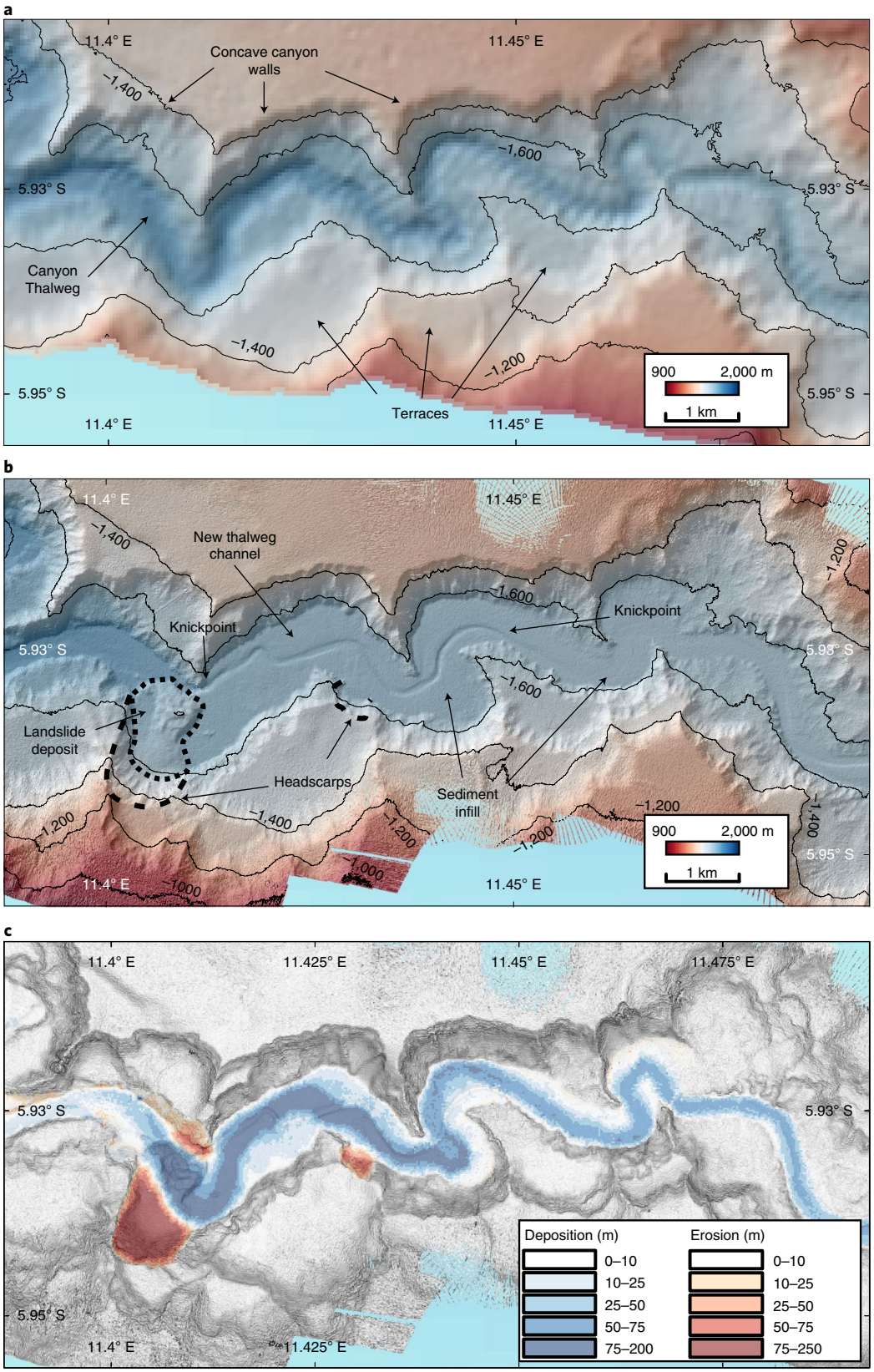

Fig. 2 | Repeat bathymetric mapping of the upper Congo Canyon and a difference map. a, Bathymetric map of part of the upper Congo Canyon derived from data collected in 2005. **b**, Bathymetric map of the same area from 2019. A canyon-flank landslide that has dammed the canyon is shown. The landslide-dam has resulted in the trapping of sediment leading to infilling up-canyon of the landslide-dam. **c**, Difference map of the 2005 data and the 2019 bathymetry resampled to 25 m showing the canyon-flank landslide, the landslide-dam and the sedimentary infill. This is overlain on a hillshade map of the 2019 bathymetric data. It allows the patterns of erosion and deposition to be characterized.

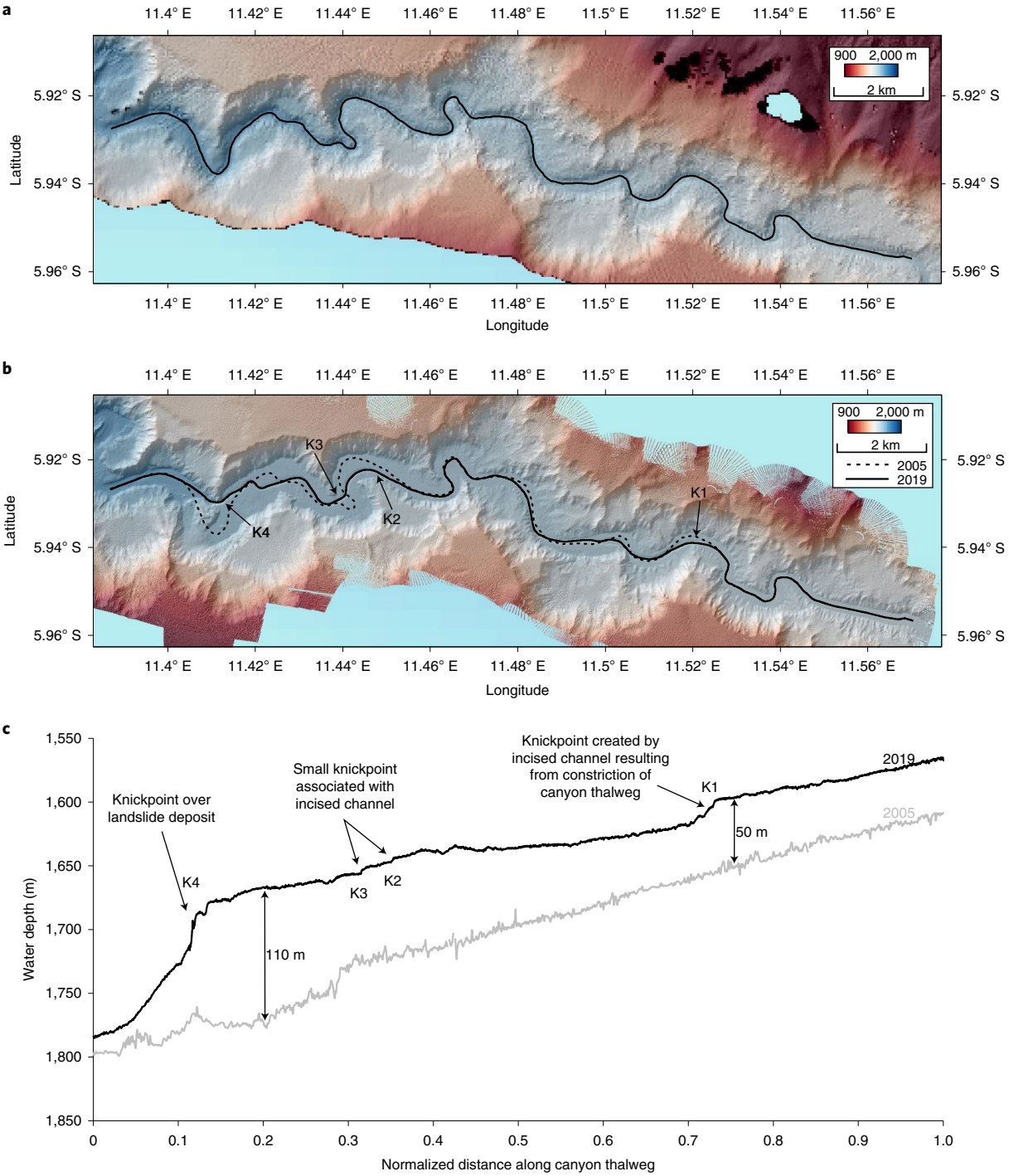

Fig. 3 | Landslide-dam impacts on the Congo Canyon thalweg. a,**b**, Plan view of the thalweg profiles in 2005 (**a**) and 2019 (**b**). Knickpoints (K1–K4) identified in **c** are shown in **b**. **c**, Thalweg profiles normalized for distance for 2005 and 2019. The profiles show the large amount of infill that has occurred post-canyon-flank collapse. The 2019 profile also shows the presence of four new knickpoints. The largest knickpoint (K4) is situated where the newly incised channel descends over the landslide-dam. The smallest knickpoints (K2 and K3) represent the up-canyon initiation of the small channel visible in Fig. 2b. The proximal knickpoint (K1) is the result of a further channel incising into the infill where the canyon is most constricted.

studies have shown that the canyon is highly active, with multiple long-duration (up to a week) turbidity currents traversing the canyon annually[8,32–34].

Bathymetric surveys of the upper canyon were conducted in 2005 and 2019 using Kongsberg EM120 and EM122 instruments. Survey design and water depths resulted in optimum gridding of these datasets at 25 m and 5 m, respectively (Methods). The contrasting dataset gridding prevents small-scale changes (<25 m) from being confidently resolved. However, large-scale changes to canyon morphology can be assessed confidently. Comparison of these datasets shows significant morphological change has occurred over ~14 years (Fig. 2). These data show that a large landslide occurred on the southern canyon flank at 1,200 m water depth (Fig. 2b). The landslide headscarp has a perimeter of 2.5 km, a maximum width

of 1 km and height of 390 m. The length of the associated deposit is ~800 m. Overall, the landslide is 1.7 km long, with an area of ~0.64 km^2. The minimum excavated volume was ~0.09 ± 0.01 km^3. A smaller landslide (0.006 ± 0.001 km^3) also occurred ~2 km up-canyon (Fig. 2b).

The canyon-flank landslide deposit caused a meander-bend cut-off, which shortened the thalweg length by ~3 km. Up-canyon of the flank collapse, canyon infilling occurred. The deposited infill is up to 150 m thick closest to the landslide deposit (Fig. 2c). At the eastern edge of the survey area, 26 km up-canyon, the newly deposited infill is up to 40 m thick. The total sediment infill volume, excluding the landslide deposit, is ~0.4 ± 0.1 km^3. A new channel has been incised into the infill (Fig. 2b). This channel is up to 20 m deep and 100 m wide and runs 6.2 km up-canyon of the landslide deposit. A series of knickpoints are associated with the landslide deposit and sediment infill. A 30-m-high knickpoint has formed where the new channel descends over the northwest end of the landslide deposit (Figs. 2b and 3). Two smaller knickpoints are also present where channels have incised into the sediment infill (Fig. 3). Down-canyon of the landslide deposit, a wedge of sediment with a volume of 0.02 ± 0.01 km^3 has been deposited.

Geomorphic change driven by canyon-flank landslides

Our data provide an opportunity to (1) test whether submarine landslide-dams may have comparable (or different) impacts to their subaerial counterparts; (2) derive models of canyon-flank landslide impacts on submarine canyon evolution and geomorphology (Fig. 4) and (3) identify the sedimentary signature of such events.

On land, where landslides block river channels, meander cut-offs have been observed where the river is forced to incise a new channel through the deposited material[14,18,35]. Sediment aggradation behind the landslide-dam can protect the channel bed, leading to slower bedrock incision rates, thereby impacting long-term longitudinal river profile evolution[17,19]. This disequilibrium can also lead to knickpoint formation as the channel adjusts to the perturbation[14,36].

Our data document a similar process in submarine canyons (Figs. 4 and 5). Where canyon-flank landslides are sufficiently large, landslide-dams can be emplaced across the canyon floor (Fig. 4b (top)). Once emplaced, this material can lead to rapid canyon infilling as sediment carried by perturbed and decelerating turbidity currents is trapped behind the dam, starving down-canyon areas of sediment (Fig. 4b (middle)). Our data show that deposition also occurs, immediately, down-canyon of the dam. This is probably a consequence of over-spilling turbidity currents that no longer have sufficient velocities to maintain sediment in suspension (Fig. 5). Once infilling has occurred, the observed new channel shows subsequent turbidity current activity can begin to erode through the landslide-dam and the infill (Figs. 2b and 4b (bottom)). We envisage that this channel was formed by erosion from the landslide-dam knickpoint once the accommodation space behind the landslide-dam was sufficiently full, such that changes in seafloor gradient did not impact the flows and allowed turbidity currents to maintain their driving force (sediment load). The rate of future channel incision and knickpoint migration will depend on turbidity current magnitude-frequency and infill-consolidation rate. The long-term existence of the observed knickpoints will depend on the incision rate through the landslide deposit and infill. Incision of a new canyon thalweg can lead to terrace formation on the canyon floor (Fig. 4b (bottom)). Where canyon-flank landslides occur on a meander bend, incision of a new thalweg channel through the infill can result in meander-bend cut-off (Fig. 3). Indeed, our observations show the first documented meander cut-off caused by a submarine canyon-flank landslide. Sediment trapped behind the dam may be gradually released by smaller flows or eroded en masse by a larger canyon-flushing event[20,37,38]. On active margins, large earthquakes may trigger a canyon-flushing event[37,38]. However, on passive margins, an alternative trigger will probably be required. In the Congo Canyon, this may be an exceptional river flood.

Where landslides are not sufficiently large or mobile enough to block terrestrial rivers or submarine canyons, we also see parallels[14]. Partial infilling of river channels is known to cause increased erosion and meander migration[14,36]. In submarine canyons (Extended Data Fig. 1b), three possible processes are envisaged (Fig. 4a,c). First, canyon-floor constriction can increase turbidity-current confinement (Fig. 4c (top)). This confinement can increase the flow's erosive potential, allowing the generation of scours and eventually the formation of a new incised channel[39]. This channel can further concentrate flows, resulting in up-canyon and down-canyon channel growth (Fig. 4c (bottom)). Second, the thalweg may be deflected. In this case, a more sinuous course would persist until the landslide deposit was eroded. Third, the landslide deposit may be too small to impact flow characteristics in the canyon thalweg. In this case, the deposit provides sediment that can be eroded by turbidity currents[21]. These smaller failures may be particularly prevalent in certain settings, such as seismically active regions where earthquakes may trigger frequent smaller-magnitude slope failures, thus reducing the frequency of canyon-damming events[40].

Landslide-dams and the resulting infill should be recognizable in submarine settings. The landslide deposit itself will be resolvable in seismic cross section as a zone of chaotic reflectors/transparency that may also have evidence of folding, normal faulting or compression[41] (Fig. 4b). Where a new thalweg has been cut post-infill, these features will probably be preserved as part of a terrace and buried beneath layered sediments (Fig. 4b (bottom)). Landslide-dams and their infill may also be recognizable from the presence of stepped changes in terrace height along a canyon, representative of the up-canyon extent of infilling resulting from the landslide-dam (Fig. 5).

Deep-sea sediment transport and submarine landslide-dams

Fluvial landslide-dams can result in the storage of large volumes of water and sediment[14]. Similarly, the observed ≥0.09 km^3 (~120 ± 10 Mt assuming a wet density of 1,800 kg m^{-3}) canyon-flank landslide-dam in the Congo Canyon has resulted in the trapping and storage of a large sediment volume (≥0.4 km^3, equivalent to ~170 ± 40 Mt assuming a wet density of 1,300 kg m^{-3}). Indeed, the volume of stored sediment could be much larger as it is still 40 m thick at the edge of the 2019 survey (Fig. 3). The annual sediment flux from the Congo River is estimated to be ~43 Mt (ref. [4]), while ref. [33] calculates ~40 Mt is transported annually by turbidity currents in the canyon. The landslide occurred at some point between 2005

Fig. 4 | Schematic model of possible morphological changes caused by large canyon-flank landslides and their stratigraphic signature. a,**b**, Morphological evolution if canyon-flank landslide dams the canyon. **a**,**c**, Morphological evolution if canyon-flank landslide constricts the canyon. **a**, Canyon walls are eroded and undercut by turbidity currents. **b**, Undercutting results in canyon-flank landslide that dams the canyon (top). Up-canyon of the landslide-dam, the canyon floor is infilled by trapped sediment transported by turbidity currents (middle). A knickpoint incises up-canyon, forming a new thalweg channel as a consequence of turbidity-current activity (bottom). The position of this new channel can lead to meander-bend cut-off and the formation of terraces. The channel may eventually erode to the pre-landslide base level. **c**, Undercutting results in a canyon-flank landslide that constricts the canyon-floor width (top). The constriction results in enhanced turbidity-current erosion and the development of a newly incised canyon-floor channel (middle). Headward erosion of a new knickpoint and continued down-canyon incision results in the growth of this new channel (bottom).

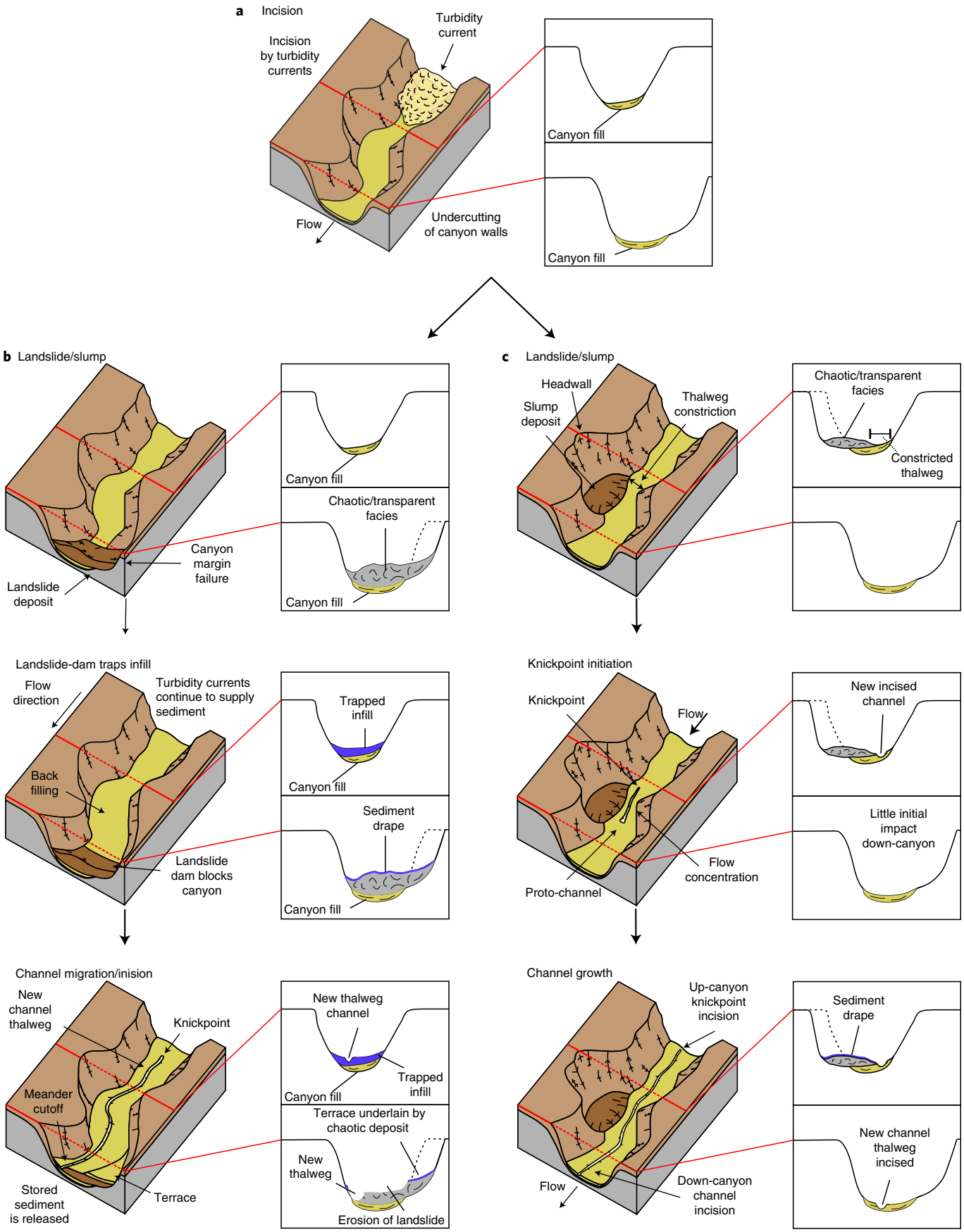
a Incision
Incision by turbidity currents
Turbidity current
Flow
Undercutting of canyon walls
Canyon fill
Canyon fill
b Landslide/slump
Landslide deposit
Canyon margin failure
Canyon fill
Chaotic/transparent facies
Canyon fill
c Landslide/slump
Headwall
Slump deposit
Thalweg constriction
Chaotic/transparent facies
Constricted thalweg
Landslide-dam traps infill
Flow direction
Turbidity currents continue to supply sediment
Back filling
Landslide dam blocks canyon
Trapped infill
Canyon fill
Sediment drape
Canyon fill
Knickpoint initiation
Knickpoint
Flow
Proto-channel
Flow concentration
New incised channel
Little initial impact down-canyon
Channel migration/inision
New channel thalweg
Knickpoint
Meander cutoff
Stored sediment is released
Terrace
New thalweg channel
Trapped infill
Canyon fill
Terrace underlain by chaotic deposit
New thalweg
Erosion of landslide
Channel growth
Up-canyon knickpoint incision
Flow
Down-canyon channel incision
Sediment drape
New channel thalweg incised

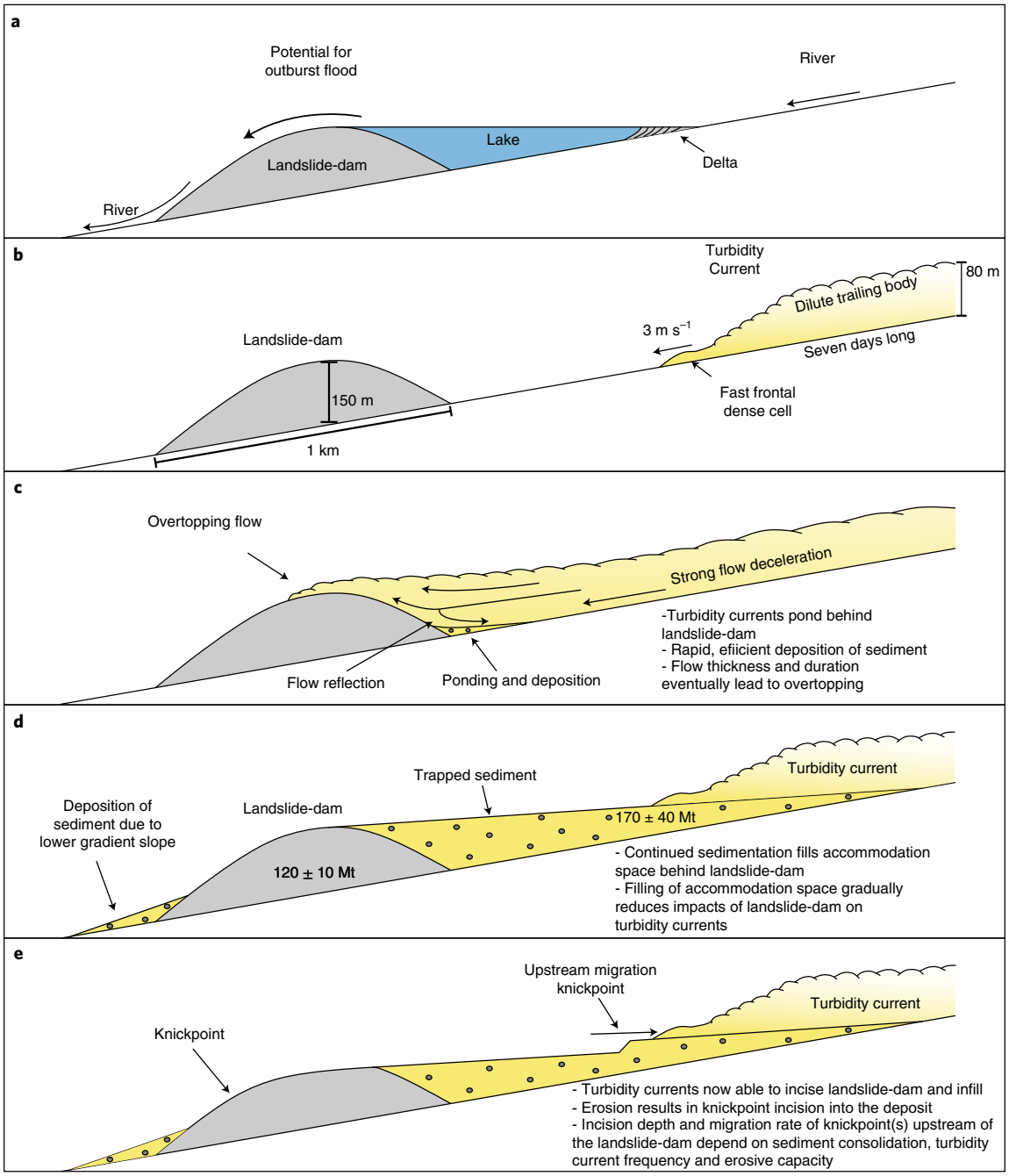

Fig. 5 | Schematic model comparing landslide-dam impacts on rivers and turbidity currents in submarine canyons. a, Terrestrial landslide-dammed river. Fluvial landslide-dam traps water and sediment. Trapped water forms a lake behind the dam, and deltaic sediment is deposited when river water enters the lake or within the body of the lake. Once accommodation space has been filled, river water is able to overtop the dam and continue downstream. **b**, Submarine landslide-dam. Landslide-dam blocks the submarine canyon, interrupting the passage of turbidity currents. **c**, Partial flow reflection and ponding. Landslide-dam results in trapping, ponding and reflection of turbidity currents. **d**, Turbidity current deposits backfill accommodation space behind landslide-dam. As turbidity currents depend on their velocity to keep sediment entrained, this sediment is rapidly deposited. Parts of the turbidity current that are able to overtop the landslide-dam quickly dissipate as their sediment load is now greatly reduced. **e**, Gradual sediment release. Once the accommodation space is filled, more-erosive, faster-moving parts of turbidity currents are able to overtop the dam. These are able to erode the dam, leading to knickpoint formation as a new channel is incised into the infill. Turbidity current in panel **b** is a scaled representation of the flows described in ref. [8] under a CC BY license.

and 2019. The landslide-dam is therefore efficiently trapping and storing large volumes of sediment that would otherwise have been transported down-canyon.

Quantifying global submarine landslide magnitude-frequency remains challenging because so few repeat multibeam bathymetry surveys have been collected. Subaerial landslide-dams can be studied and dated far more easily, especially with the advent of remote-sensing techniques[14]. The largest inventory of subaerial landslide-dams contains >1,000 examples since 1900[14]. In this Article, we show the scale of this Congo Canyon landslide-dam

and sediment infill is comparable to the largest terrestrial examples. Despite their frequent occurrence globally, only 24 fluvial landslide-dams since 1900 have volumes >0.09 km^3, and only 40 have dammed lake volumes >0.4 km^3. The Congo landslide-dam is equivalent to the 98th percentile for volume and 95th percentile for stored volumes in this 120 yr subaerial inventory.

The key differentiator between subaerial and submarine landslide-dams is how sediment is stored. Initially, fluvial landslide-dams will trap water and sediment. Once filled, sediment may continue to be deposited as the river enters the dammed lake, but water is still able to overtop the dam and continue to erode and transport sediment downstream[13–18]. By contrast, submarine landslide-dams will result in rapid infilling of sediment, and starve down-canyon reaches of sediment, due to the trapping of turbidity currents by the dam. Unlike rivers, turbidity currents in submarine channels are driven by their sediment load, and their ability to keep sediment entrained depends on their velocity[8]. Turbidity currents that deposit sediment lose driving force, potentially leading to further deceleration and sediment deposition; this positive feedback does not occur in rivers. Recent monitoring studies[7,8,33] have suggested that turbidity currents are driven by dense, near-bed frontal cells (Fig. 5b). These dense frontal cells will probably be retained behind the dam, perturbing the flow and potentially resulting in flow ponding and reflection, leading to rapid deposition[42]. Only when the accommodation space is sufficiently filled will parts of the turbidity current pass over the landslide-dam[42] (Fig. 5c,d). However, the loss of sediment still leads to further deposition immediately down-canyon, reducing turbidity-current run-out. Once filled, further turbidity-current activity will rework the infill (Figs. 2b and 5e).

Submarine landslide-dams and OC sequestration

Burial of young OC, produced by photosynthesis in the biosphere, in marine sediments removes CO_2 from the atmosphere, regulating the climate over geological timescales[26]. Indeed, submarine canyons are considered efficient sequesters of OC in the ocean[23,26,27]. However, few measurements of OC sequestration exist in these environments, and we are therefore yet to constrain long-term fluxes or burial efficiencies despite common submarine canyon occurrence on all continental margins.

Measurements of sediment from the Congo Fan averaged over multiple sampling locations[29] suggest a total OC content estimated at 2.75–3.00% by weight[29]. Assuming such values, the canyon-flank landslide and trapped infill contained ~3.2–3.5 and ~4.6–5.0 Mt of OC, respectively. The landslide will re-exhume already buried OC, but the infill is likely to contain younger OC[43]. The Congo River annually supplies ~2 Mt terrestrial OC (Supplementary Table 2). The buried OC therefore represents a minimum of 3–4 years of terrestrial OC supply from the river and ~4% of the global total of OC delivered annually by rivers to the oceans[5]. Thus, although worldwide frequency-magnitude of landslide-dams in submarine canyons is uncertain, this single example buried 4% of the terrestrial OC flux to the global ocean (Supplementary Table 2).

The rapid burial (<14 years) of this mass of OC should prevent oxidation and thus preserve the OC. This supports the previous assertions that submarine canyons are effective carbon sinks[23,26,27]. However, subsequent reworking by turbidity currents of OC stored in the dammed wedge of sediment will probably expose much of this carbon to future oxidation. The OC drawdown, therefore, depends on the preservation of terraces after a new channel has been incised into the infill. A similar process is envisaged for the re-exhumed OC contained in the landslide deposit. Erosion and re-exhumation are intrinsic to a meandering channel, but recurrent mass sliding, as suggested by the identified landslide, and concave canyon walls (Figs. 1 and 2) clearly add to the amount of re-exhumation. This suggests that landslides and landslide-dams probably reduce the efficiency of OC burial in canyons and their perceived role as efficient carbon sinks.

The mass of OC buried in the Congo Canyon infill is comparable to that remobilized by the Tohoku-oki and Kaikōura earthquakes[11,44]. These earthquakes resulted in ~1.7 and ~7.0 Mt OC being remobilized, respectively. Delivery of OC to the deep sea by these and other earthquake-triggered events is believed to exert a strong control over regional deep-sea productivity and carbon sequestration[11,44]. By contrast, landslide-dams will temporally lead to reduced OC fluxes that nourish down-system benthic ecosystems[45–47]. Submarine canyon-damming therefore has the potential to modulate marine carbon transport and cycling. These impacts will probably be greater where canyons are directly connected to terrestrial sediment sources. However, landslide-dams in canyons that are starved of terrestrial inputs may also exert impacts on OC cycling due to the impacts on ecosystems that rely on down-canyon sediment transport[1].

We identified a submarine landslide-dam that is comparable in scale to the largest landslide-dams of the past 120 years. It shows how submarine landslide-dams may affect sediment and OC transfer to the deep sea and submarine canyon geomorphic evolution. This single example had a comparable impact on sediment and OC fluxes to the deep sea as major earthquakes and trapped a sediment mass four times the annual flux from the Congo River, equivalent to ~4% of the annual supply of terrestrial OC to the global oceans. Similar landslide scars are commonplace on the flanks of other submarine canyons (Supplementary Table 1), including those connecting to very large rivers[48,49]. This suggests submarine landslide-dams could potentially be common phenomena, even away from active margins. Indeed, at least three other landslide-dams have been identified in modern bathymetry (Supplementary Table 1). However, time-lapse bathymetric surveys are currently available for only ~4 of the ~9,477 submarine canyons known globally. This study shows the value of repeat high-resolution bathymetric mapping of large deep-sea systems. Further work should now determine the frequency of submarine landslide-damming to constrain their impact on deep-sea ecosystems, sediment transport and OC burial on different margin types.

Online content

Any methods, additional references, Nature Research reporting summaries, source data, extended data, supplementary information, acknowledgements, peer review information; details of author contributions and competing interests; and statements of data and code availability are available at https://doi.org/10.1038/s41561-022-01017-x.

Received: 27 January 2021; Accepted: 26 July 2022;
Published online: 29 September 2022

References

1. Harris, P. T. & Whiteway, T. Global distribution of large submarine canyons: geomorphic differences between active and passive continental margins. *Mar. Geol.* **285**, 69–86 (2011).
2. Maier, K. L. et al. Submarine-fan development revealed by integrated high-resolution datasets from La Jolla Fan, offshore California, USA. *J. Sediment. Res.* **90**, 468–479 (2020).
3. Covault, J. A., Fildani, A., Romans, B. W. & McHargue, T. The natural range of submarine canyon-and-channel longitudinal profiles. *Geosphere* **7**, 313–332 (2011).
4. Milliman, J. D. & Farnsworth, K. L. *River Discharge to the Coastal Ocean: A Global Synthesis* (Cambridge Univ. Press, 2011).
5. Galy, V., Peucker-Ehrenbrink, B. & Eglinton, T. Global carbon export from the terrestrial biosphere controlled by erosion. *Nature* **521**, 204–207 (2015).
6. Guiastrennec-Faugas, L. et al. Upstream migrating knickpoints and related sedimentary processes in a submarine canyon from a rare 20-year morphobathymetric time-lapse (Capbreton submarine canyon, Bay of Biscay, France). *Mar. Geol.* **423**, 106143 (2020).

7. Paull, C. K. et al. Powerful turbidity currents driven by dense basal layers. *Nat. Commun.* **9**, 4114 (2018).
8. Azpiroz-Zabala, M. et al. Newly recognised turbidity current structure can explain prolonged flushing of submarine canyons. *Sci. Adv.* **3**, e1700200 (2017).
9. Guiastrennec-Faugas, L. et al. Initiation and evolution of knickpoints and their role in cut-and-fill processes in active submarine channels. *Geology* (2020).
10. Hughes Clarke, J. E., Marques, C. R. V. & Pratomo, D. in *Advances in Natural and Technological Hazards Research* 249–260 (Springer, 2014).
11. Mountjoy, J. J. et al. Earthquakes drive large-scale submarine canyon development and sediment supply to deep-ocean basins. *Sci. Adv.* **4**, eaar3748 (2018).
12. Korup, O. Recent research on landslide dams—a literature review with special attention to New Zealand. *Prog. Phys. Geog.* **26**, 206–235 (2002).
13. Schuster, R. L. Landslide dams—a worldwide phenomenon. *J. Jpn Landslide Soc.* **31**, 38–49 (1995).
14. Fan, X. et al. The formation and impact of landslide dams–state of the art. *Earth Sci. Rev.* **203**, 103116 (2020).
15. Costa, J. E. & Schuster, R. L. The formation and failure of natural dams. *Geol. Soc. Am. Bull.* **100**, 1054–1068 (1988).
16. Dunning, S. A., Rosser, N. J., Petley, D. N. & Massey, C. R. Formation and failure of the Tsatichhu landslide dam, Bhutan. *Landslides* **3**, 107–113 (2006).
17. Ouimet, W. B., Whipple, K. X., Royden, L. H., Sun, Z. & Chen, Z. The influence of large landslides on river incision in a transient landscape: eastern margin of the Tibetan Plateau (Sichuan, China). *Geol. Soc. Am. Bull.* **119**, 1462–1476 (2007).
18. Fan, X. et al. Transient water and sediment storage of the decaying landslide dams induced by the 2008 Wenchuan earthquake, China. *Geomorphology* **171**, 58–68 (2012).
19. Korup, O. Rock-slope failure and the river long profile. *Geology* **34**, 45–48 (2006).
20. Piper, D. J. W. & Normark, W. R. Processes that initiate turbidity currents and their influence on turbidites: a marine geology perspective. *J. Sediment. Res.* **79**, 347–362 (2009).
21. Mountjoy, J. J., Barnes, P. M. & Pettinga, J. R. Morphostructure and evolution of submarine canyons across an active margin: Cook Strait sector of the Hikurangi Margin, New Zealand. *Mar. Geol.* **260**, 45–68 (2009).
22. Babonneau, N., Savoye, B., Cremer, M. & Klein, B. Morphology and architecture of the present canyon and channel system of the Zaire deep-sea fan. *Mar. Pet. Geol.* **19**, 445–467 (2002).
23. Galy, V. et al. Efficient organic carbon burial in the Bengal fan sustained by the Himalayan erosional system. *Nature* **450**, 407–410 (2007).
24. Rabouille, C. et al. Carbon and silica megasink in deep-sea sediments of the Congo terminal lobes. *Quat. Sci. Rev.* **222**, 105854 (2019).
25. Kane, I. A. et al. Seafloor microplastic hotspots controlled by deep-sea circulation. *Science* **368**, 1140–1145 (2020).
26. Hage, S. et al. Efficient preservation of young terrestrial organic carbon in sandy turbidity-current deposits. *Geology* https://doi.org/10.1130/g47320.1 (2020).
27. Masson, D. G. et al. Efficient burial of carbon in a submarine canyon. *Geology* **38**, 831–834 (2010).
28. McClain, C. R. & Barry, J. P. Habitat heterogeneity, disturbance, and productivity work in concert to regulate biodiversity in deep submarine canyons. *Ecology* **91**, 964–976 (2010).
29. Baudin, F., Rabouille, C. & Dennielou, B. Routing of terrestrial organic matter from the Congo River to the ultimate sink in the abyss: a mass balance approach (André Dumont medallist lecture 2017). *Geol. Belgica* https://doi.org/10.20341/gb.2020.004 (2020).
30. Babonneau, N., Savoye, B., Cremer, M. & Bez, M. Sedimentary architecture in meanders of a submarine channel: detailed study of the present Congo turbidite channel (Zaiango project). *J. Sediment. Res.* **80**, 852–866 (2010).
31. Babonneau, N., Savoye, B., Cremer, M. & Bez, M. Multiple terraces within the deep incised Zaire Valley (ZaïAngo Project): are they confined levees? *Geol. Soc. Lond. Spec. Publ.* **222**, 91–114 (2004).
32. Vangriesheim, A., Khripounoff, A. & Crassous, P. Turbidity events observed in situ along the Congo submarine channel. *Deep Sea Res. Part 2* **56**, 2208–2222 (2009).
33. Simmons, S. M. et al. Novel acoustic method provides first detailed measurements of sediment concentration structure within submarine turbidity currents. *J. Geophys. Res. Oceans* **125**, e2019JC015904 (2020).
34. Khripounoff, A. et al. Direct observation of intense turbidity current activity in the Zaire submarine valley at 4000 m water depth. *Mar. Geol.* **194**, 151–158 (2003).
35. Gong, J. et al. Impacts of the Wenchuan Earthquake on the Chaping River upstream channel change. *Int. J. Remote Sens.* **33**, 3907–3929 (2012).
36. Korup, O. Effects of large deep-seated landslides on hillslope morphology, western Southern Alps, New Zealand. *J. Geophys. Res. Earth Surf.* **111**, F01018 (2006).
37. Canals, M. et al. Flushing submarine canyons. *Nature* **444**, 354–357 (2006).
38. Allin, J. R. et al. Different frequencies and triggers of canyon filling and flushing events in Nazaré Canyon, offshore Portugal. *Mar. Geol.* **379**, 89–105 (2016).
39. Gee, M. J. R., Masson, D. G., Watts, A. B. & Mitchell, N. C. Passage of debris flows and turbidity currents through a topographic constriction: seafloor erosion and deflection of flow pathways. *Sedimentology* **48**, 1389–1409 (2001).
40. ten Brink, U. S., Geist, E. L. & Andrews, B. D. Size distribution of submarine landslides and its implication to tsunami hazard in Puerto Rico. *Geophys. Res. Lett.* **33**, L11307 (2006).
41. Hampton, M. A., Lee, H. J. & Locat, J. Submarine landslides. *Rev. Geophys.* **34**, 33–59 (1996).
42. Kneller, B. C. & Buckee, C. The structure and fluid mechanics of turbidity currents: a review of some recent studies and their geological implications. *Sedimentology* **47**, 62–94 (2000).
43. Baudin, F. et al. Organic carbon accumulation in modern sediments of the Angola basin influenced by the Congo deep-sea fan. *Deep Sea Res. Part 2* **142**, 64–74 (2017).
44. Kioka, A. et al. Megathrust earthquake drives drastic organic carbon supply to the Hadal Trench. *Sci. Rep.* **9**, 1553 (2019).
45. Guerra, M. et al. Changes in habitat use by a deep-diving predator in response to a coastal earthquake. *Deep Sea Res. Part 1* **158**, 103226 (2020).
46. Fernandez-Arcaya, U. et al. Ecological role of submarine canyons and need for canyon conservation: a review. *Front. Mar. Sci.* https://doi.org/10.3389/fmars.2017.00005 (2017).
47. Sen, A. et al. Fauna and habitat types driven by turbidity currents in the lobe complex of the Congo deep-sea fan. *Deep Sea Res. Part 2* **142**, 167–179 (2017).
48. Li, Y. et al. Continuous Holocene input of river sediment to the Indus Submarine Canyon. *Mar. Geol.* **406**, 159–176 (2018).
49. Curray, J. R., Emmel, F. J. & Moore, D. G. The Bengal Fan: morphology, geometry, stratigraphy, history and processes. *Mar. Pet. Geol.* **19**, 1191–1223 (2002).

Methods

The results presented in this paper are based on analysis of bathymetry data of the upper Congo Canyon collected during cruises JC187 of the RRS *James Cook* (2019) and OPTIC-CONGO2 in 2005 on board the FS *Beautemps-Beaupré*. JC187 used a Kongsberg EM122 system, and OPTIC-CONGO2 used a Kongsberg EM120. Both operated at 12 kHz with a vertical sounding accuracy of 0.2% of water depth. The beam aperture was 0.5° × 0.5° for JC187 and 1° × 1° for OPTIC-CONGO2. Data were processed to correct for differences in sound velocity in the water column (using data from sound-velocity profilers) and the ship's motion. JC187 data were processed in CARIS HIPS and SIPS software and gridded with a resolution of 5 m. JC187 data were able to be gridded at 5 m due to the high number of soundings that were retrieved due to the survey design. The canyon was surveyed using along-canyon lines crossed by traverse lines perpendicular to the along-canyon lines to minimize potential shadowing or reflection due to steep canyon walls. The survey paths were also designed to ensure the entire survey area was covered by the central third of the swath width to maximize the number of soundings. The OPTIC-CONGO2 survey used along-canyon lines. OPTIC-CONGO2 data were processed and gridded at 25 m in CARAIBES. Inter-survey positioning was validated by matching features in common areas of relatively stable seafloor.

Erosion and deposition of sediment between 2005 and 2019 were calculated by first resampling the JC187 5 m data to 25 m so as to be comparable with the OPTIC-CONGO2 data. A bathymetric difference map produced in ArcGIS was subsequently used to determine volumes of eroded and deposited sediment. Where canyon-flank landslides were observed, their volumes were calculated using depth changes associated with their headwalls. This was necessary because the emplaced deposit was often buried, and no seismic data penetrating the landslide deposits were available, preventing direct assessment of the deposit volume. The calculated landslide volumes are therefore probably only minimum volumes.

The bathymetric surveys were used to construct along-canyon profiles. The position of submarine canyon and channel thalwegs shift as they evolve, so down-canyon profiles were measured along the position of the thalweg in each survey. These profiles were subsequently normalized for comparison in the section of the canyon impacted by the canyon-flank landslide and infill. Normalized distances along canyon were calculated by taking a starting point (Fig. 3; furthest point west) where the thalweg was in the same location for both surveys and dividing each measurement of distance by the distance travelled along the thalweg to the end point of the profiles (Fig. 3; furthest point east).

The morphology of the Congo Submarine Canyon observed in the JC187 and OPTIC-CONGO2 bathymetry data was also compared with high-resolution bathymetric data that has been previously published for a range of submarine canyons around the world[6,11,50–85] (Supplementary Table 1). The volumes of sediment and OC stored in-canyon and up-canyon of the observed landslide-dam were also compared with a range of known events in marine and fluvial environments in terms of displaced masses and OC transport[5,11,29,44,86–98] (Supplementary Table 2).

Data availability

We do not own the rights to make the JC187 or OPTIC-CONGO2 datasets available. However, access to each dataset can be requested following these instructions. Requests for the multibeam data from JC187 should be made to the British Oceanographic Data Centre (BODC; https://www.bodc.ac.uk/). Access or requests for the multibeam data compiled on the Congo Fan, including the OPTIC-CONGO2 cruise, should be made through the Sextant Portal at Ifremer (https://doi.org/10.12770/d1076601-82a9-42a2-9d30-d0be8b2481a7).

References

50. Aiello, G., Iorio, M., Molisso, F. & Sacchi, M. Integrated morpho-bathymetric, seismic-stratigraphic, and sedimentological data on the Dohrn Canyon (Naples Bay, Southern Tyrrhenian Sea): relationships with volcanism and tectonics. *Geosciences* **10**, 319 (2020).
51. Amundsen, H. B. et al. Late Weichselian–Holocene evolution of the high-latitude Andøya submarine Canyon, North-Norwegian continental margin. *Mar. Geol.* **363**, 1–14 (2015).
52. Laberg, J. S. et al. Morphology and morphogenesis of a high-latitude canyon; the Andøya Canyon, Norwegian Sea. *Mar. Geol.* **246**, 68–85 (2007).
53. Antobreh, A. A. & Krastel, S. Morphology, seismic characteristics and development of Cap Timiris Canyon, offshore Mauritania: a newly discovered canyon preserved-off a major arid climatic region. *Mar. Pet. Geol.* **23**, 37–59 (2006).
54. Baztan, J. et al. Axial incision: the key to understand submarine canyon evolution (in the western Gulf of Lion). *Mar. Pet. Geol.* **22**, 805–826 (2005).
55. Bernhardt, A. et al. Controls on submarine canyon activity during sea-level highstands: the Biobío canyon system offshore Chile. *Geosphere* **11**, 1226–1255 (2015).
56. Biscara, L. et al. Morphological evolution of Cap Lopez (Gabon): illustration of lateral migration processes of a submarine canyon. *Mar. Geol.* **340**, 49–56 (2013).
57. Casalbore, D. et al. in *Subaqueous Mass Movements and Their Consequences: Advances in Process Understanding, Monitoring and Hazard Assessments* (eds Georgiopoulou, A. et al.) 393–403 (Geological Society London, 2022).
58. de Almeida, N. M., Vital, H. & Gomes, M. P. Morphology of submarine canyons along the continental margin of the Potiguar Basin, NE Brazil. *Mar. Pet. Geol.* **68**, 307–324 (2015).
59. Gardner, J. A., Armstrong, A. A. & Calder, B. R. Hatteras transverse canyon, Hatteras Outer Ridge and the environs of the US Atlantic margin: a view from multibeam bathymetry and backscatter. *Mar. Geol.* **371**, 18–32 (2016).
60. Green, A. & Uken, R. Submarine landsliding and canyon evolution on the northern KwaZulu-Natal continental shelf, South Africa, SW Indian Ocean. *Mar. Geol.* **254**, 152–170 (2008).
61. Green, A. Submarine canyons associated with alternating sediment starvation and shelf-edge wedge development: northern KwaZulu-Natal continental margin, South Africa. *Mar. Geol.* **284**, 114–126 (2011).
62. Harris, P. T, Barrie, J. V, Conway, K. W & Greene, H. G. Hanging canyons of Haida Gwaii, British Columbia, Canada: fault-control on submarine canyon geomorphology along active continental margins. *Deep Sea Res. Part 2* **104**, 83–92 (2014).
63. Jimoh, R. O. et al. The architecture of the lower parts of submarine canyons on the western Nigerian continental margin. *Acta Oceanol. Sin.* **37**, 28–40 (2018).
64. Lastras, G. et al. A walk down the Cap de Creus canyon, northwestern Mediterranean Sea: recent processes inferred from morphology and sediment bedforms. *Mar. Geol.* **246**, 176–192 (2007).
65. Clift, P. D., Giosan, L., Henstock, T. J. & Tabrez, A. R. Sediment storage and reworking on the shelf and in the canyon of the Indus River-Fan System since the last glacial maximum. *Basin Res.* **26**, 183–202 (2014).
66. Li, Y., Clift, P. D. & O'Sullivan, P. Millennial and centennial variations in zircon U–Pb ages in the Quaternary Indus submarine canyon. *Basin Res.* **31**, 155–170 (2019).
67. Yeh, Y. -C. et al. *Seafloor Morphology and Slope Failures of the Kaoping Canyon Upstream Area* (Taiwan Ocean Research Institute, 2013).
68. Liu, J. T. et al. From the highest to the deepest: the Gaoping River–Gaoping Submarine Canyon dispersal system. *Earth Sci. Rev.* **153**, 274–300 (2016).
69. Lo Iacono, C. et al. Submarine canyon morphologies in the Gulf of Palermo (Southern Tyrrhanian Sea) and possible implications for geo-hazard. *Mar. Geophys. Res.* **32**, 127–138 (2011).
70. Micallef, A. et al. in *Submarine Mass Movements and their Consequences* (eds Yamada, Y. et al.) 201–212 (Springer, 2013).
71. Micallef, A. et al. Space-for-time substitution and the evolution of a submarine canyon-channel system in a passive progradational margin. *Geomorphology* **221**, 34–50 (2014).
72. Mondziel, S., Grindlay, N., Mann, P., Escalona, A. & Abrams, L. Morphology, structure, and tectonic evolution of the Mona canyon (northern Mona passage) from multibeam bathymetry, side-scan sonar, and seismic reflection profiles. *Tectonics* **29**, TC2003 (2010).
73. Nanson, R. A. et al. Cretaceous to Cenozoic controls on the genesis of the shelf-incising Perth Canyon; insights from a two-part geomorphology mapping approach. *Mar. Geol.* **445**, 106731 (2022).
74. Normandeau, A. et al. Morphodynamics in sediment-starved inner-shelf submarine canyons (Lower St. Lawrence Estuary, Eastern Canada). *Mar. Geol.* **347**, 243–255 (2014).
75. Oiwane, H. et al. Geomorphological development of the Goto Submarine Canyon, northeastern East China Sea. *Mar. Geol.* **288**, 49–60 (2011).
76. Paull, C. K. et al. Anatomy of the La Jolla Submarine Canyon system; offshore southern California. *Mar. Geol.* **355**, 16–34 (2013).
77. Pierdomenico, M., Martorelli, E., Dominguez-Carrió, C., Gili, J. M. & Chiocci, F. L. Seafloor characterisation and benthic megafaunal distribution of an active submarine canyon and surrounding sectors: the case of Gioia Canyon (Southern Tyrrhenian Sea). *J. Mar. Syst.* **157**, 101–117 (2016).
78. Popescu, I. et al. The Danube submarine canyon (Black Sea): morphology and sedimentary processes. *Mar. Geol.* **206**, 249–265 (2004).
79. Puga-Bernabéu, A., Webster, J. M., Beaman, R. J. & Guilbaud, V. Morphology and controls on the evolution of a mixed carbonate–siliciclastic submarine canyon system, Great Barrier Reef margin, north-eastern Australia. *Mar. Geol.* **289**, 100–116 (2011).
80. Ratzov, G., Sosson, M., Collet, J.-Y. & Migeon, S. Late Quaternary geomorphic evolution of submarine canyons as a marker of active deformation on convergent margins: the example of the South Colombian margin. *Mar. Geol.* **315-318**, 77–97 (2012).
81. Rona, P. et al. Hudson submarine canyon head offshore New York and New Jersey: a physical and geochemical investigation. *Deep Sea Res. Part 2* **121**, 213–232 (2015).
82. Serra, C. S. et al. Tectonic evolution, geomorphology and influence of bottom currents along a large submarine canyon system: the São Vincente Canyon (SW Iberian margin). *Mar. Geol.* **426**, 106219 (2020).

83. Tournadour, E. et al. Submarine canyon morphologies and evolution in modern carbonate settings: the northern slope of Little Bahama Bank, Bahamas. *Mar. Geol.* **391**, 76–97 (2017).
84. Wiles, E., Green, A., Watkeys, M., Botes, R. & Jokat, W. Submarine canyons of NW Madagascar: a first geomorphological insight. *Deep Sea Res. Part 2* **161**, 5–15 (2019).
85. Paull, C. K., Caress, D. W., Ussler, W., Lundsten, E. & Meiner-Johnson, M. High-resolution bathymetry of the axial channels within Monterey and Soquel submarine canyons, offshore central California. *Geosphere* **7**, 1077–1101 (2011).
86. Leithold, E. L. & Hope, R. S. Deposition and modification of a flood layer on the northern California shelf: lessons from and about the fate of terrestrial particulate organic carbon. *Mar. Geol.* **154**, 183–195 (1999).
87. Rathburn, S. L. et al. The fate of sediment, wood, and organic carbon eroded during an extreme flood, Colorado Front Range, USA. *Geology* **45**, 499–502 (2017).
88. West, A. J. et al. Mobilization and transport of coarse woody debris to the oceans triggered by an extreme tropical storm. *Limnol. Oceanogr.* **56**, 77–85 (2011).
89. Goldsmith, S. T. et al. Extreme storm events, landscape denudation, and carbon sequestration: Typhoon Mindulle, Choshui River, Taiwan. *Geology* **36**, 483–486 (2008).
90. Coynel, A., Seyler, P., Etcheber, H., Meybeck, M. & Orange, D. Spatial and seasonal dynamics of total suspended sediment and organic carbon species in the Congo River. *Glob. Biogeochem. Cycles* **19**, GB4019 (2005).
91. Milliman, J. D. & Farnsworth, K. L. in *River Discharge to the Coastal Ocean: A Global Synthesis* 13–69 (Cambridge Univ. Press, 2011).
92. Bouchez, J. et al. Source, transport and fluxes of Amazon River particulate organic carbon: insights from river sediment depth-profiles. *Geochim. Cosmochim. Acta* **133**, 280–298 (2014).
93. Wakeham, S. G. et al. Partitioning of organic matter in continental margin sediments among density fractions. *Mar. Chem.* **115**, 211–225 (2009).
94. Rosenheim, B. E. et al. River discharge influences on particulate organic carbon age structure in the Mississippi/Atchafalaya River System. *Glob. Biogeochem. Cycles* **27**, 154–166 (2013).
95. Li, G. et al. Dam-triggered organic carbon sequestration makes the Changjiang (Yangtze) river basin (China) a significant carbon sink. *J. Geophys. Res. Biogeosci.* **120**, 39–53 (2015).
96. Galy, V., Beyssac, O., France-Lanord, C. & Eglinton, T. I. Recycling of graphite during Himalayan erosion: a geological stabilization of carbon in the crust. *Science* **322**, 943–945 (2008).
97. Galy, V. & Eglinton, T. Protracted storage of biospheric carbon in the Ganges–Brahmaputra basin. *Nat. Geosci.* **4**, 843–847 (2011).
98. Hilton, R. G. et al. Erosion of organic carbon in the Arctic as a geological carbon dioxide sink. *Nature* **524**, 84–87 (2015).

Acknowledgements

The crews and shipboard parties of the RRS *James Cook* and FS *Beatutemps-Beaupré* are thanked for their help collecting the data. We thank our partners Angola Cables and others involved in requesting and granting permissions to work in Angolan territorial waters. E.L.P. was supported by a Leverhulme Trust Early Career Fellowship (ECF-2018-267). D.R.P. acknowledges funding from EU grant no. 725955 - GEOSTICK. C.J.H. and M.S.H. acknowledge funding from EU grant no 721403 - ITN Slate. M.J.B.C. was supported by a Royal Society Research Fellowship (DHF\R1\180166). S.H. has received funding from the European Union's Horizon 2020 research and innovation programme under the Marie Skłodowska-Curie grant agreement no. 899546. We acknowledge NERC funding (NE/R001952/1, NE/S010068/1, NE/V004387/1). M.A.C. was supported by the UK National Capability NERC CLASS programme (NERC grant NE/R015953) and NERC grants (NE/P009190/1, NE/P005780/1).

Author contributions

E.L.P. wrote the manuscript with significant editing and revision from M.S.H., P.J.T., R.S.J., M.L.B., S.H., M.H., C.J.H., C.M., S.R., S.M.S., B.D., A.G., C.P., M.A.C. and M.U.

Competing interests

The authors declare no competing interests.

Additional information

Extended data is available for this paper at https://doi.org/10.1038/s41561-022-01017-x.

Supplementary information The online version contains supplementary material available at https://doi.org/10.1038/s41561-022-01017-x.

Correspondence and requests for materials should be addressed to Ed L. Pope.

Peer review information *Nature Geoscience* thanks Joshu Mountjoy, Silvia Ceramicola and the other, anonymous, reviewer(s) for their contribution to the peer review of this work. Primary Handling Editor: James Super, in collaboration with the *Nature Geoscience* team.

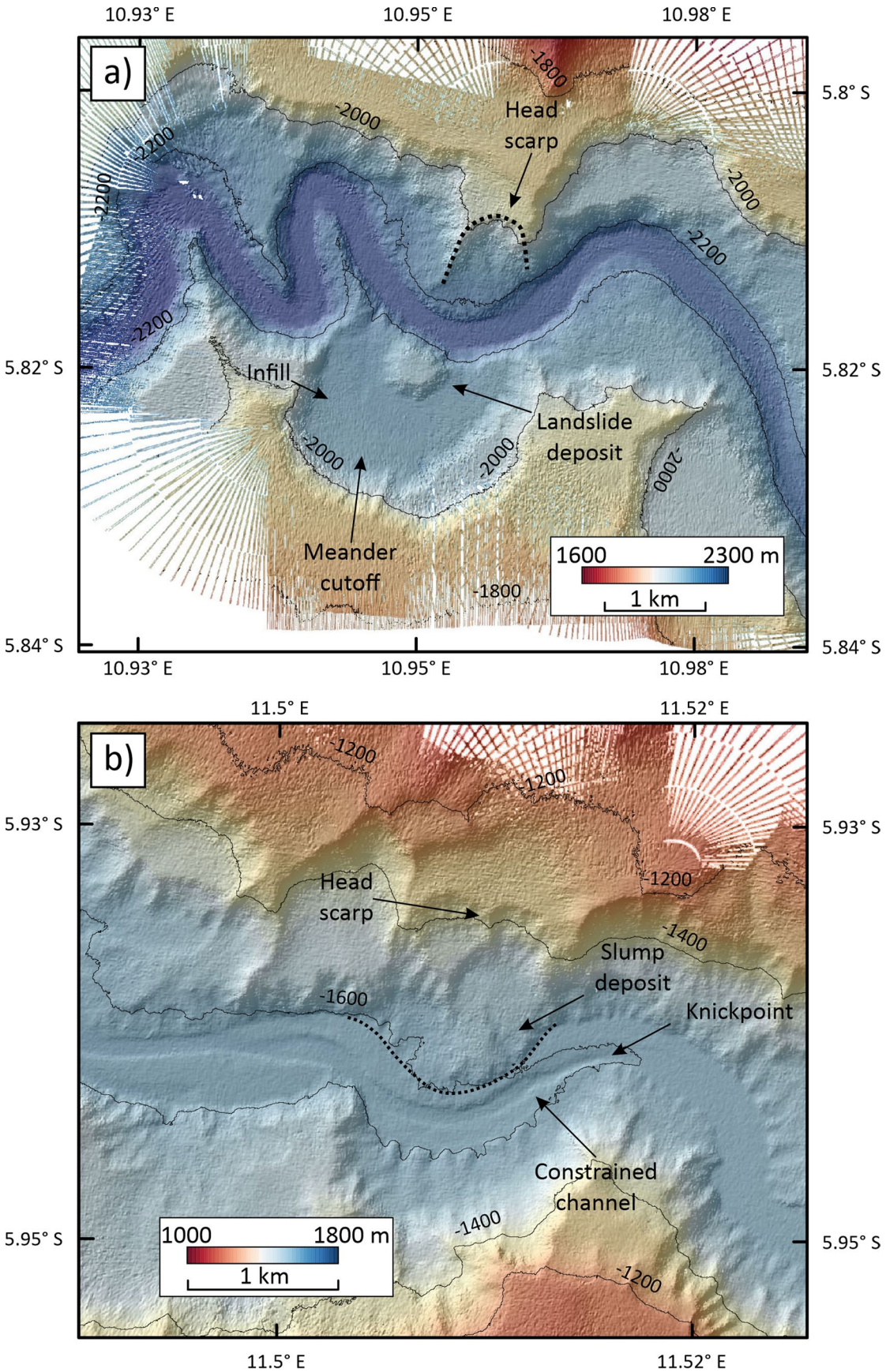

Extended Data Fig. 1 | See next page for caption.

Extended Data Fig. 1 | Two possible canyon-flank landslides identified in the 2019 bathymetry. a) Possible landslide headscarp and deposit which are interpreted to have involved similar processes to those envisaged for the canyon-flank landslide seen in Fig. 2. b) Canyon-flank landslide appears to constrict the canyon floor leading to the development of a new thalweg channel due to enhanced turbidity current erosional capacity. Processes envisaged here are similar to those described in Figs. 4a, c1-c3.